ELSEVIER

Applied Ocean Research 20 (1998) 337–355

Applied Ocean Research

Numerical simulation of sloshing waves in a 3D tank based on a finite element method

G.X. Wu[a], Q.W. Ma[a], R. Eatock Taylor[b]

[a]*Department of Mechanical Engineering, University College London, Torrington Place, London WC1E 7JE, UK*
[b]*Department of Engineering Science, University of Oxford, Parks Road, Oxford OX1 3PJ, UK*

Received 24 February 1998; accepted 8 September 1998

Abstract

The sloshing waves in a three dimensional (3D) tank are analysed using a finite element method based on the fully non-linear wave potential theory. When the tank is undergoing two dimensional (2D) motion, the calculated results are found to be in very good agreement with other published data. Extensive calculation has been made for the tank in 3D motion. As in 2D motion, in addition to normal standing waves, travelling waves and bores are also observed. It is found that high pressures occur in various circumstances, which could have important implications for many engineering designs. © 1998 Elsevier Science Ltd. All rights reserved.

Keywords: Engineering design; Numerical simulation; Finite element method; Sloshing waves

1. Introduction

Sloshing waves are associated with various engineering problems, such as the liquid oscillations in large storage tanks caused by earthquakes, the motions of liquid fuel in aircraft and spacecraft, the liquid motions in containers and the water flow on the decks of ships. The loads produced by the wave motion can cause structural damage and the loss of the motion stability of objects such as ships.

There has been a considerable amount of work on wave sloshing. For the case of small motions, Abramson [1] used a linear theory and Solaas and Faltinsen [2] adopted a perturbation theory. For large motions, Jones and Hulme [3], Faltinsen [4], Okamoto and Kawahara [5], Chen et al. [6] and Armenio and La Rocca [7] used various numerical methods for the two dimensional problem. For the three dimensional problem, Huang and Hsiung [8] used the shallow water equation for the flow on the ship deck.

This body of work has significantly advanced our knowledge about sloshing waves in a tank. It is now well understood that apart from normal standing waves, other wave forms, such as travelling waves and bores, can occur. Under certain conditions, high pressure and impact forces will be created on the side walls of the tank. This can have several serious implications such as the following:

1. high pressures may create excessive stress and deformation within the walls, so that structural failure may become more likely; and
2. for a structure such as a ship, the high pressure may create an overturning moment in roll, which could be large enough to cause capsize.

The publications mentioned above are either based on a two dimensional method or a shallow water formulation. The answers they offer to these concerns are applicable only when their adopted assumptions are valid.

In this work, the analysis is based on the three dimensional and fully non-linear potential theory in the time domain. The numerical method adopted is the finite element formulation described in detail in Wu et al. [9] and Ma et al. [10]. Although the method can be applied to a tank of an arbitrary shape and undergoing both translational motion and rotational motion, the results presented in this paper are for a rectangular tank undergoing translational motion only. The purpose here is to show how the waves behave in a practical three dimensional tank. We have provided extensive results for this reason. It has to be emphasised, however, that we do not pretend to offer a complete solution to the wave sloshing problem. In fact, the results obtained have presented us with more questions than answers, which clearly require further investigation.

In the following sections, we first briefly outline the mathematical formulation and the numerical method. The computer code is then verified by comparing the calculated results with the published two dimensional data, and

PII: S0141-1187(98)00030-3

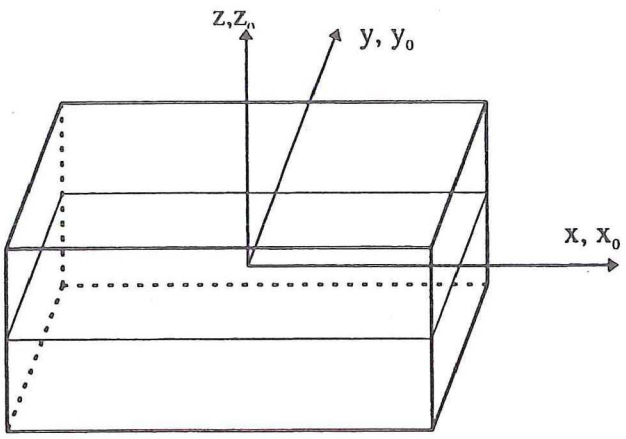

Fig. 1. The co-ordinate system.

excellent agreement is found. After that, an extensive set of calculations is made for a tank undergoing motions in more than one direction. It is particularly interesting to see that the combination of certain small excitations may create large waves in the tank.

2. Mathematical formulation

Two Cartesian co-ordinate systems are defined: one, $o_0x_0y_0z_0$ is fixed in space and the other, $oxyz$, is fixed on the tank. When the tank is at rest, the two systems coincide with each other and the origins are at the centre of the undisturbed free surface. The directions of the axes are as shown in Fig. 1.

The displacements of the tank in the directions of the Cartesian axes are defined as:

$$X_b = [x_b(t),\ y_b(t),\ z_b(t)] \tag{1}$$

Based on potential flow theory, the velocity potential ϕ satisfies the Laplace equation:

$$\nabla^2\phi = 0 \tag{2}$$

On the side walls of the tank, the potential satisfies:

$$\frac{\partial\phi}{\partial n} = \boldsymbol{U}\cdot\boldsymbol{n} \tag{3}$$

where $\boldsymbol{U} = \dfrac{d\boldsymbol{X}_b}{dt}$ is the velocity of the tank and n is outward vector normal to the tank walls. On the free surface, $z_0 = \zeta_0(x_0, y_0, t)$, the dynamic and kinematic conditions in the space fixed system can be written as:

$$\frac{\partial\phi}{\partial t} + \frac{1}{2}\nabla\phi\cdot\nabla\phi + g\zeta_0 = 0 \tag{4}$$

$$\frac{\partial\zeta_0}{\partial t} + \frac{\partial\phi}{\partial x_0}\frac{\partial\zeta_0}{\partial x_0} + \frac{\partial\phi}{\partial y_0}\frac{\partial\zeta_0}{\partial y_0} - \frac{\partial\phi}{\partial z_0} = 0 \tag{5}$$

The free surface elevation can be more easily described in the moving system. Thus if we use:

$$\nabla_{x_0y_0z_0} = (\nabla)_{xyz} \tag{6}$$

$$\left(\frac{\partial}{\partial t}\right)_{x_0y_0z_0} = \left(\frac{\partial}{\partial t} - \frac{d\boldsymbol{X}_b}{\partial t}\cdot\nabla\right)_{xyz} \tag{7}$$

Eqs. (4) and (5) become:

$$\frac{\partial\phi}{\partial t} - \nabla\phi\cdot\frac{d\boldsymbol{X}_b}{\partial t} + \frac{1}{2}\nabla\phi\cdot\nabla\phi + g(\zeta + z_b) = 0 \tag{8}$$

$$\frac{\partial\zeta}{\partial t} + \left(\frac{\partial\phi}{\partial x} - \frac{dx_b}{dt}\right)\frac{\partial\zeta}{\partial x} + \left(\frac{\partial\phi}{\partial y} - \frac{dy_b}{dt}\right)\frac{\partial\zeta}{\partial y} - \left(\frac{\partial\phi}{\partial z} - \frac{dz_b}{dt}\right) = 0 \tag{9}$$

on $z = \zeta$, where $\zeta = \zeta_0 - z_b$ is the free surface elevation in the moving system $oxyz$ For fixed x and y, the change of the potential with time on the free surface is governed by

$$\frac{\delta\phi[x, y, \zeta(x, y, t), t]}{\delta t} = \frac{\partial\phi}{\partial t} + \frac{\partial\phi}{\partial z}\frac{\partial\zeta}{\partial t} \tag{10}$$

where $\dfrac{\partial\phi}{\partial t}$ is the same term as in Eq. (8). The dynamic condition on the free surface then becomes:

$$\frac{\partial\phi}{\partial t} + \frac{\partial\phi}{\partial z}\frac{\partial\zeta}{\partial t} - \nabla\phi\cdot\frac{d\boldsymbol{X}_b}{\partial t} + \frac{1}{2}\nabla\phi\cdot\nabla\phi + g(\zeta + z_b) = 0 \tag{11}$$

The velocity potential, ϕ, can now be split as follows:

$$\phi = \varphi + xu + yv + zw \tag{12}$$

where u, v and w are the components of $\boldsymbol{U}$ in the x, y and z directions, respectively. Substituting this equation into Eq.

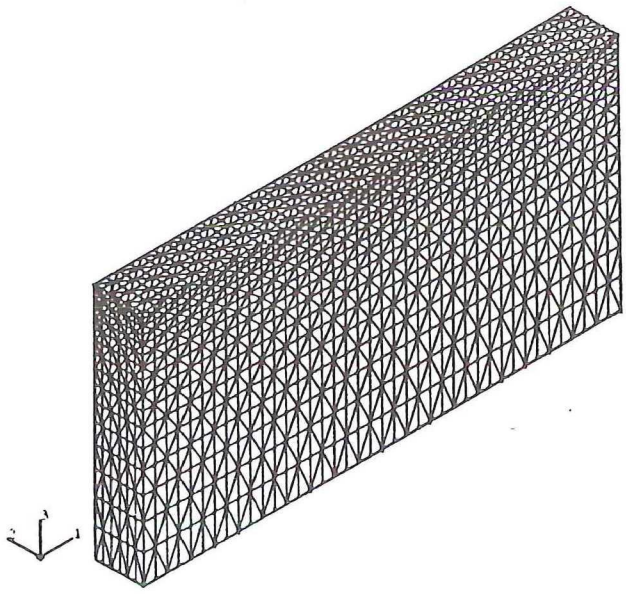

Fig. 2. Initial mesh for sloshing wave.

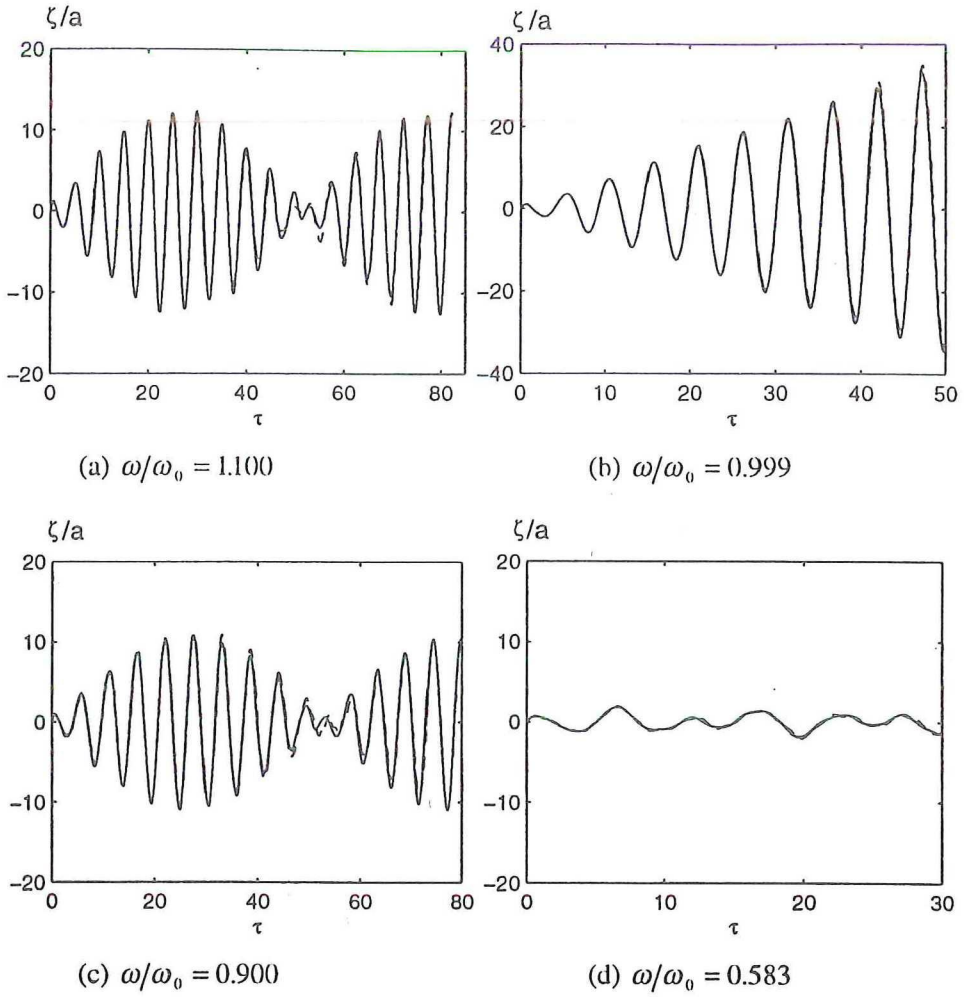

Fig. 3. Time history of free surface elevation at $x = -L/2$ for different frequencies (solid line: analytical; dashed line: numerical). (a) $\omega/\omega_0 = 1.100$; (b) $\omega/\omega_0 = 0.999$; (c) $\omega/\omega_0 = 0.900$; (d) $\omega/\omega_0 = 0.583$.

(2), Eq. (3), Eq. (9) and Eq. (11), we have:

$$\nabla^2\varphi = 0 \text{ in the fluid} \tag{13}$$

$$\frac{\partial\varphi}{\partial n} = 0 \text{ on the side walls} \tag{14}$$

$$\frac{\partial\zeta}{\partial t} = -\frac{\partial\varphi}{\partial x}\frac{\partial\zeta}{\partial x} - \frac{\partial\varphi}{\partial y}\frac{\partial\zeta}{\partial y} + \frac{\partial\varphi}{\partial z} \text{ on the free surface} \tag{15}$$

$$\frac{\delta\varphi}{\delta t} = \frac{\partial\varphi}{\partial z}\frac{\partial\zeta}{\partial t} - \frac{1}{2}\nabla\varphi\cdot\nabla\varphi - g\zeta - x\frac{du}{dt} - y\frac{dv}{dt} - \zeta\frac{dw}{dt} \text{ on the free surface} \tag{16}$$

where the term $c(t) = \frac{1}{2}|U|^2 - gz_b$ has been deleted from Eq. (16) because it is independent of the spatial coordinates.

These equations need to be combined with initial conditions, which are usually given as:

$$\phi(x_0, y_0, 0, 0) = 0 \tag{17}$$

$$\zeta_0(x_0, y_0, 0) = 0 \tag{18}$$

This means that:

$$\varphi(x, y, 0, 0) = -xu(0) - yv(0) \tag{19}$$

$$\zeta(x, y, 0) = 0 \tag{20}$$

Once the solution has been found at one time step, Eq. (15) and Eq. (16) can be used to obtain the new wave elevation and the new potential on the free surface, which will be used as the boundary conditions at the next time step.

The pressure in the fluid can be obtained from:

$$-\frac{p}{\rho} = \left(\frac{\partial\phi}{\partial t} + \frac{1}{2}\nabla\phi\cdot\nabla\phi + gz\right)_{x_0y_0z_0}$$

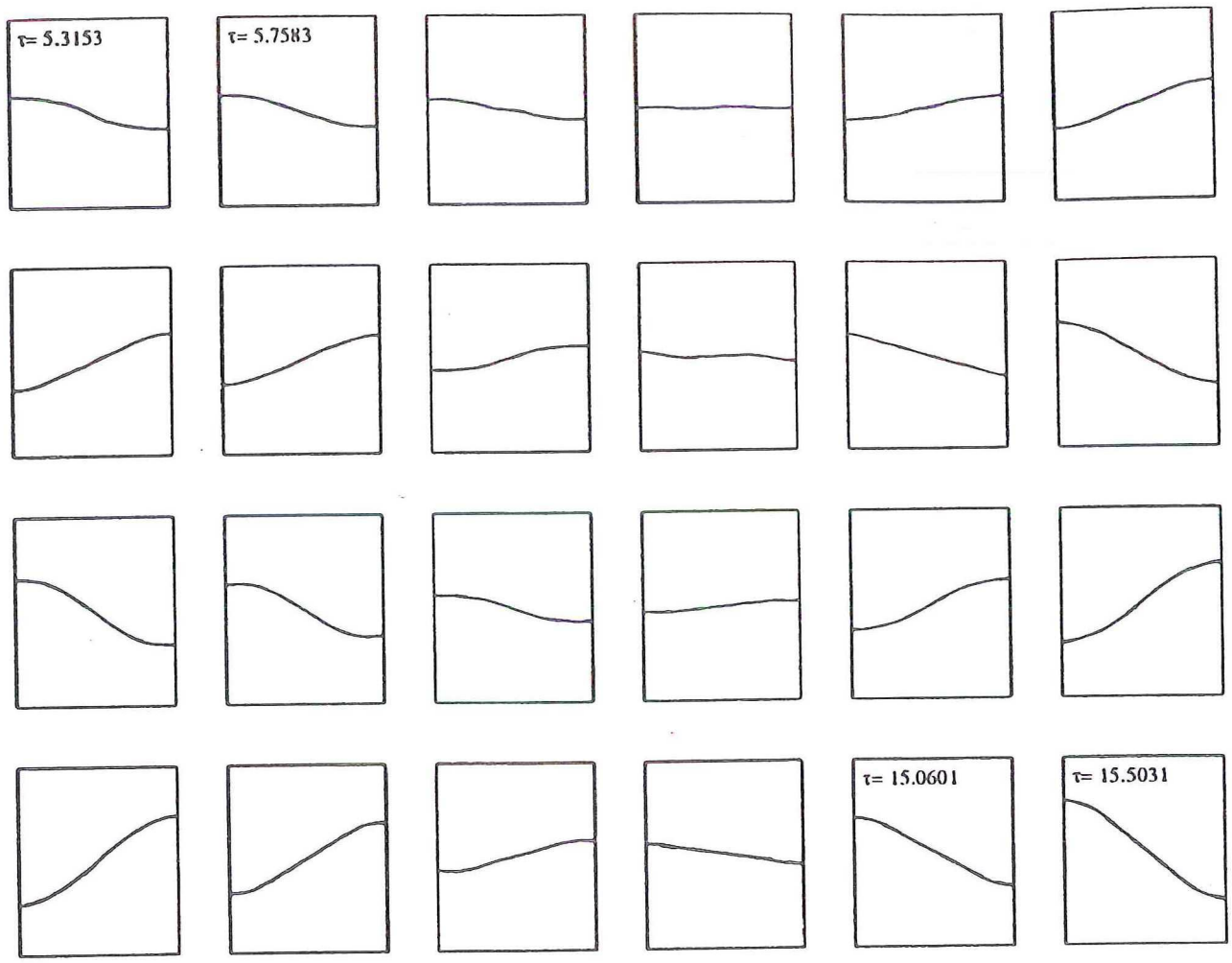

Fig. 4. Free surface profiles for $\omega/\omega_0 \approx 0.999$ (solid line: analytical; dashed line: numerical).

If Eq. (7) and Eq. (12) are used this becomes:

$$-\frac{p}{\rho} = \frac{\partial \varphi}{\partial t} + \frac{1}{2}\nabla\varphi\cdot\nabla\varphi + gz + x\frac{du}{dt} + y\frac{dv}{dt} + \zeta\frac{dw}{dt} \quad (21)$$

3. Finite element formulation and numerical procedure

The above problem can be solved based on a finite element formulation [9]. In general, the velocity potential can be written as:

$$\varphi = \sum_{j=1}^{J_N} \varphi_j N_j(x,y,z) \quad (22)$$

where J_N is the total number of nodes, $N_j(x,y,z)$ are the shape functions and φ_j are the values of the potential at the nodes. Using the Galerkin method and Green's second identity and taking into account the body surface boundary condition in Eq. (14), we have

$$\iiint_{\Omega} \nabla N_i \sum_{\substack{j=1 \\ j\notin S_f}}^{J_N} \varphi_j \nabla N_j d\Omega = -\iiint_{\Omega} \nabla N_i \sum_{\substack{j=1 \\ j\in S_f}}^{J_N} \varphi_j \nabla N_j \, d\Omega \quad i \notin S_f \quad (23)$$

where S_f indicates the free surface and Ω is the fluid domain. The solution of this equation can then be obtained by an iterative procedure [10] and the following scheme is employed for the integration over the time:

$$f(t+\Delta t) = f(t) + \frac{\Delta t}{2}[3f'(t) - f'(t-\Delta t)] \quad (24)$$

where $f'(t)$ represents the temporal derivative.

4. Numerical results

4.1. Two dimensional cases

We consider a case in which the displacement of the tank is governed by $x_b(t) = a\sin(\omega t)$, $y_b = 0$ and $z_b = 0$ when $t >$

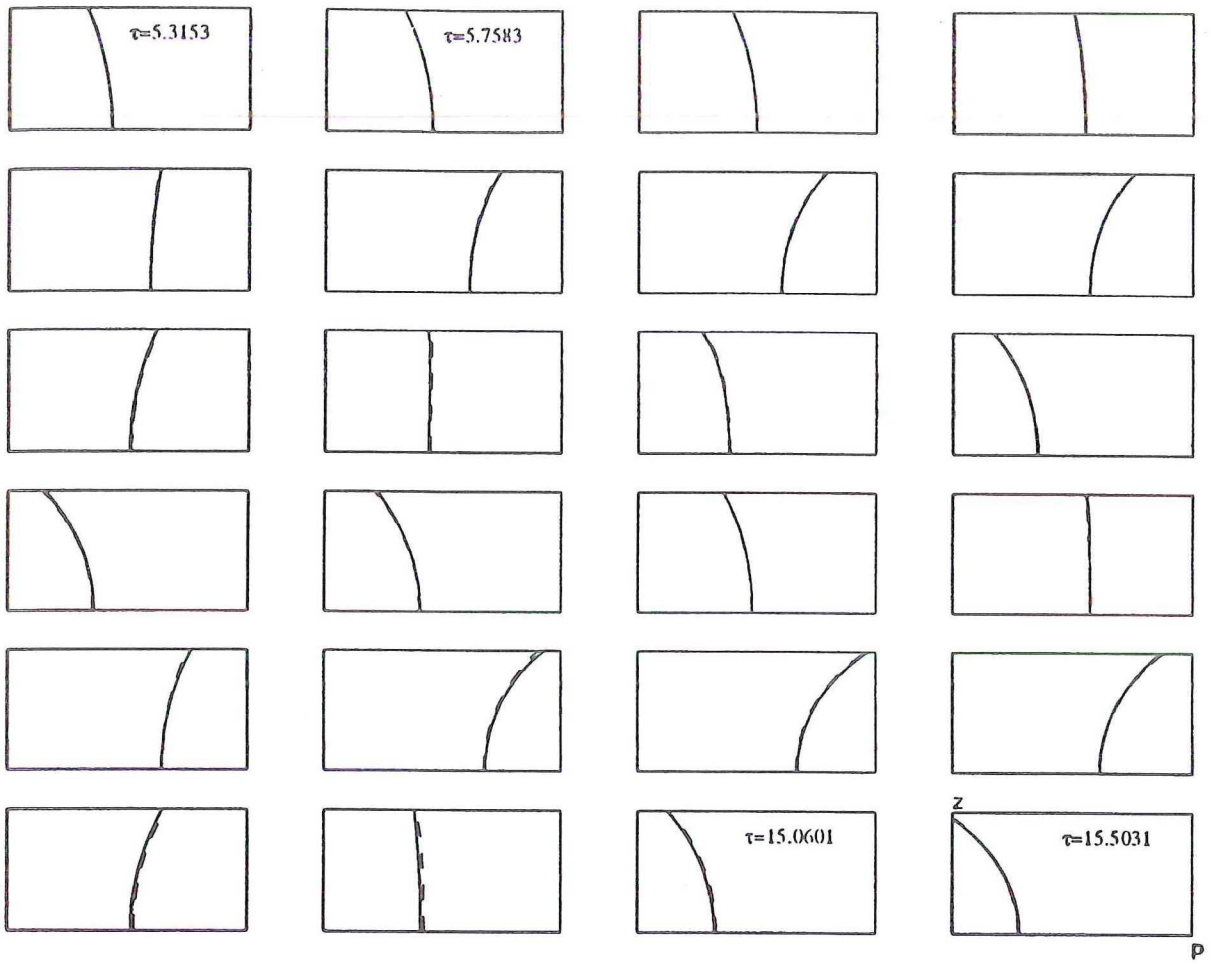

Fig. 5. Comparison of numerical pressure along the water depth ($x = L/2$, $y = 0$) for $\omega/\omega_0 \approx 0.999$ with analytical solution (Solid line: analytical solution; dashed line: numerical simulation).

0, where a is the amplitude and ω is the frequency. The corresponding velocity is $u = a\omega\cos(\omega t)$, and $v = w = 0$. The initial condition of the problem is given in Eqs. (19) and (20). This two-dimensional case has been investigated by many people, e.g. Faltinsen [4], Okamoto and Kawahara [5] and Chen et al. [6]. Their results may be used here for comparison. The dimensions of the tank are chosen as $L/d = 2.0$ and $B/d = 0.2$ where L, B and d are the length,

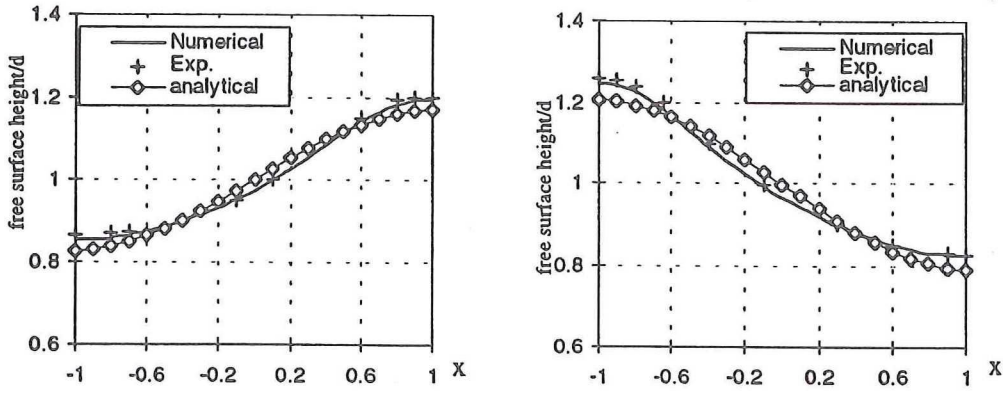

(a) $\tau = 13.0667$ (b) $\tau = 15.725$

Fig. 6. Comparison of free surface elevation with experimental data. (a) $\tau = 13.0667$; (b) $\tau = 15.725$.

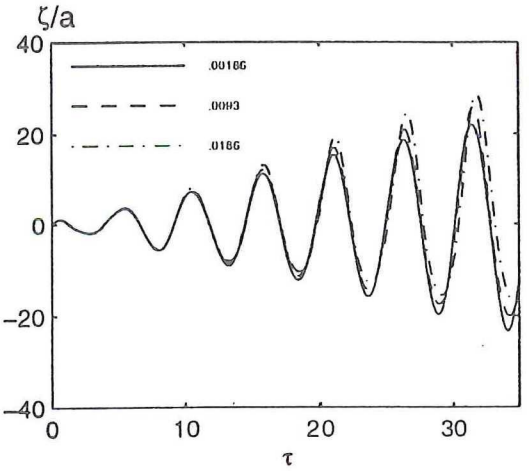

(a) Wave history ($x = -L/2$) ($a = 0.00186, 0.0093, 0.0186$)

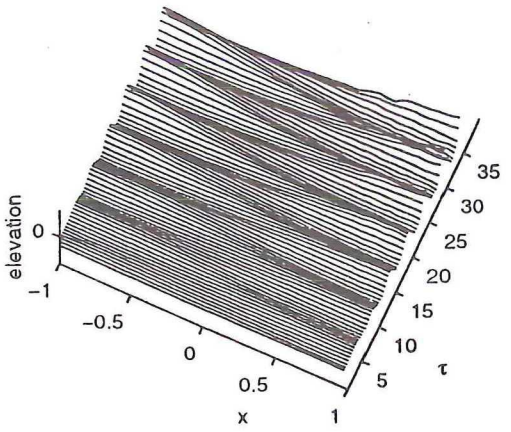

(b) Wave profile, $a = 0.0186$

Fig. 7. Wave history and profile for $\chi = 0.5$.

the width and the water depth, respectively, (the same as those used in the experiment by Okamoto and Kawahara [5]). A linearised solution for φ can easily be found from the results of Faltinsen [4]:

$$\varphi = a\sum_{n=0}^{\infty}\left(C_n\cos\omega t - \left(C_n + \frac{H_n}{\omega^2}\right)\cos\omega_n t\right) \times \frac{\cosh k_n(z+d)}{\cosh k_n d}\sin k_n x \tag{25}$$

where

$$k_n = \frac{2n+1}{L}\pi,\ \omega_n^2 = gk_n\tanh k_n d,$$

$$H_n = \omega^3\frac{4}{L}\frac{4(-1)^n}{k_n^2} \text{ and } C_n = \frac{H_n}{\omega_n^2 - \omega^2}.$$

The dynamic pressure and the wave elevation can then be obtained from:

$$p = -\rho g\left(\frac{\partial\varphi}{\partial t} + x\frac{du}{dt}\right) \tag{26}$$

$$\zeta = \zeta_1 + \zeta_2 \tag{27}$$

where

$$\zeta_1 = \frac{a}{g}\left(x\omega^2 + \sum_{n=0}^{\infty} C_n\omega\sin k_n x\right)\sin\omega t$$

$$\zeta_2 = -\frac{a}{g}\sum_{n=0}^{\infty}\omega_n\left(C_n + \frac{H_n}{\omega^2}\right)\sin k_n x\,\sin\omega_n t.$$

In the numerical analysis, the fluid domain is first divided into hexahedra using N horizontal planes through the water depth, M_1 vertical planes perpendicular to the x-axis and M_2 vertical planes perpendicular to the y-axis. Each of these hexahedra is then split into six tetrahedra. A typical initial mesh is illustrated in Fig. 2.

In the analysis below, some parameters are nondimensionalized as follows:

$$(x, y, z, L, B, a) \to (x, y, z, L, B, a)d,\ t \to \tau\sqrt{\frac{d}{g}},$$
$$\omega \to \omega\sqrt{\frac{g}{d}},\ k \to \frac{k}{d} \tag{28}$$

To compare with the linear analytical results, the numerical simulation is carried out with a small amplitude $a = 0.00186$. The excitation frequency is either higher or lower than the first natural frequency $\omega_0 = \sqrt{k_0\tanh k_0 d}$. In the calculation, we have chosen $M_1 = 40$, $M_2 = 6$, $N = 16$ and $\Delta\tau = 0.0111$, which has been found to give converged results (see the next section for details). The time history of the free surface at $x = -L/2$ is presented in Fig. 3. Comparison between the analytical solution and the numerical results shows that they are in an excellent agreement.

It is interesting to see from Fig. 3(a) and Fig. 3(c) that the wave history is very similar to that due to two harmonic wave trains of slightly different frequencies. This amplitude modulated wave can be understood from Eq. (27). The expression is composed of two parts: one corresponds to the excitation frequency ω and the other corresponds to the natural frequencies ω_0, ω_1, ω_2, ω_3,.... Of the latter, the wave of the first frequency ω_0 is dominant and others have far less contribution. As a result, the entire wave is actually dominated by two waves of frequencies ω and ω_0. As is well known, the frequency of the envelope of the amplitude-modulated wave is $\Delta\omega = |\omega - \omega_0|$ and its time

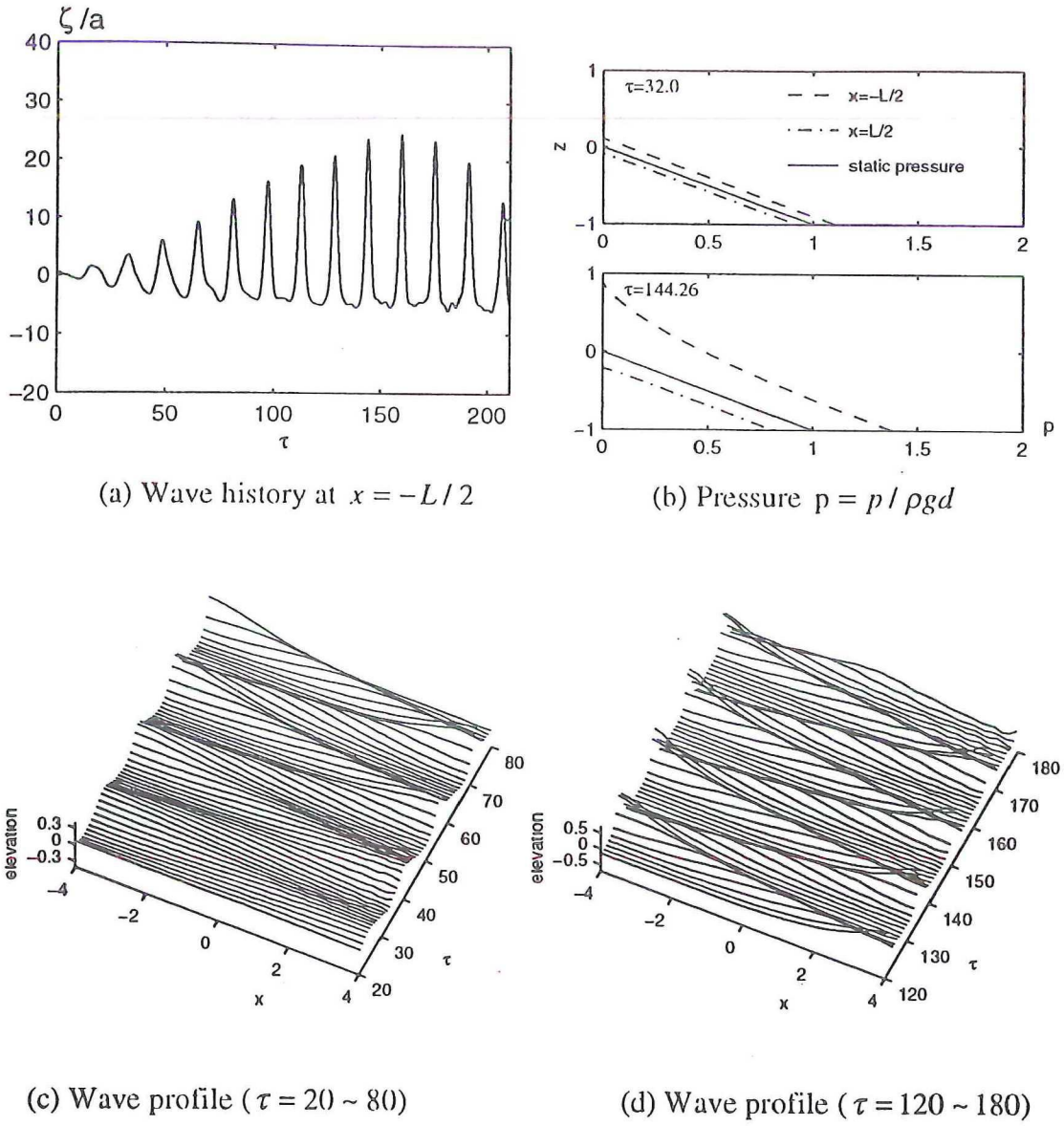

(a) Wave history at $x = -L/2$ (b) Pressure $p = p/\rho gd$

(c) Wave profile ($\tau = 20 \sim 80$) (d) Wave profile ($\tau = 120 \sim 180$)

Fig. 8. Wave history, profile and pressure ($\omega = 0.9998\omega_a$, $a = 0.0372$).

Table 1
The cases for three-dimensional sloshing

Case	Dimension		Frequency			Amplitude		
	L	B	ω_x	ω_y	ω_z	a_x	a_y	a_z
A	4	4	.9999 ω_{0x}	.9999 ω_{0y}	0.0	0.372×10^{-3}	0.372×10^{-3}	0.0
B	4	4	.9999 ω_{0x}	.9999 ω_{0y}	0.0	0.0372	0.0372	0.0
C	4	4	.9995 ω_{1x}	.9995 ω_{1y}	0.0	0.0186	0.0186	0.0
D[a]	4	4			2.04 ω_{0x}			0.2
E	4	4	.9995 ω_{1x}	.9995 ω_{1y}	2.04 ω_{0x}	0.0186	0.0186	0.2
F	8	8	.9999 ω_{0x}	.9999 ω_{0y}	0.0	0.0372	0.0372	0.0
G	8	4	.9999 ω_{0x}	.9999 ω_{0y}	0.0	0.0372	0.0186	0.0
H	25	25	.998 ω_{0x}	.998 ω_{0y}	0.0	1.2	1.2	0.0

[a] Horizontal velocity disturbance is applied only at $\tau = 0$ [see Eq. (25)].

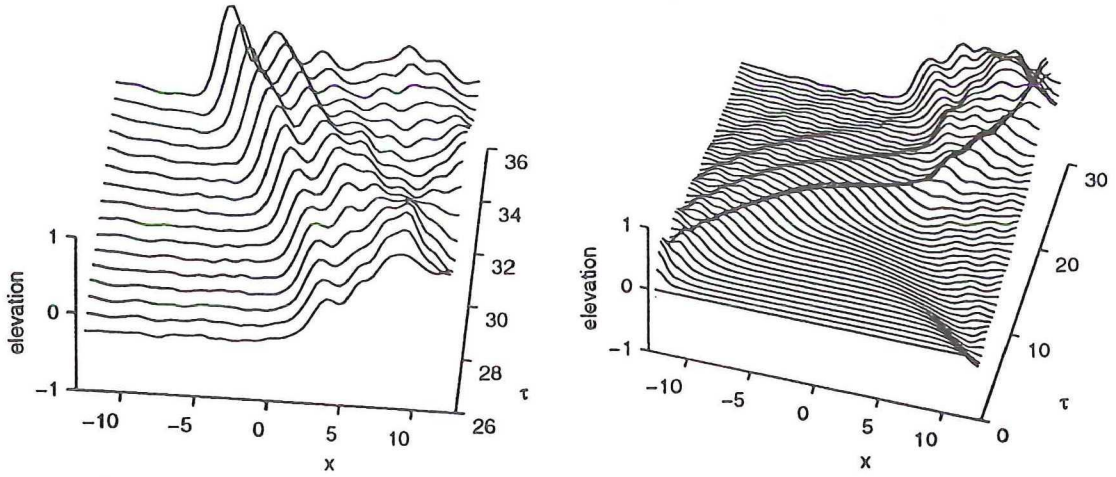

Fig. 9. Wave profile for $a = 2.5$ and $\omega = 0.9973\omega_0$.

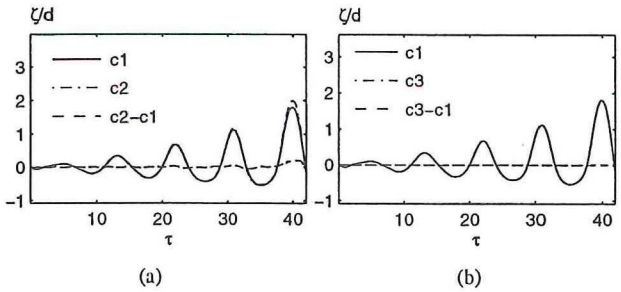

Fig. 10. Comparison of wave elevation history at ($L/2$, $B/2$) for different meshes and time steps.

period is $2\pi/\Delta\omega$, which can clearly be seen in Fig. 3(a) and Fig. 3(c) ($2\pi/\Delta\omega \approx 52.25$ from the linear theory).

One can see from Fig. 3(b) that the wave amplitude increases with time. Indeed, the magnitude of ζ/a has reached around 30 at $\tau \approx 50$. However, it does not of course suggest that the amplitude will tend to infinity with time, even based on the linear theory. The result is due to $\Delta\omega$ being very small, which leads to a very long period ($2\pi/\Delta\omega \approx 6283$) and a very large amplitude of the wave envelope.

Fig. 4 shows 'snapshots' of the free surface profiles between $\tau = 5.3153$ and $\tau = 15.5031$, at intervals equal to 0.443, for the case of $\omega/\omega_0 \approx 0.999$. Fig. 5 gives corresponding comparisons of the numerical pressure with the analytical solution through the water depth. Again a good

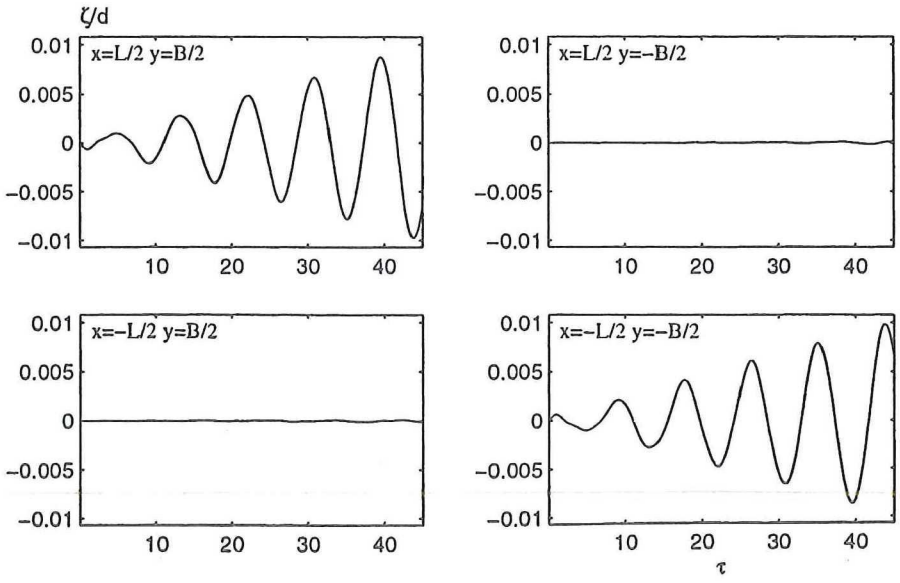

Fig. 11. Wave elevation history at four corners (Case A).

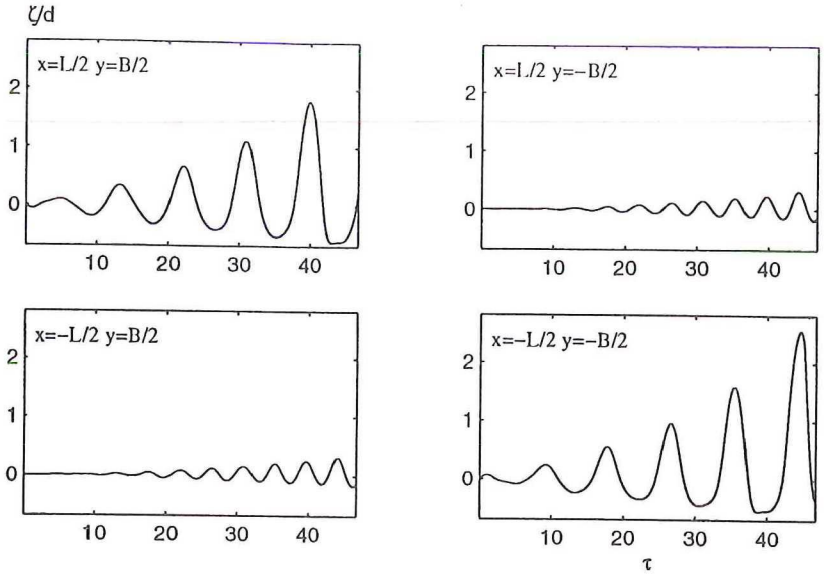

Fig. 12. Wave elevation history at four corners (Case B).

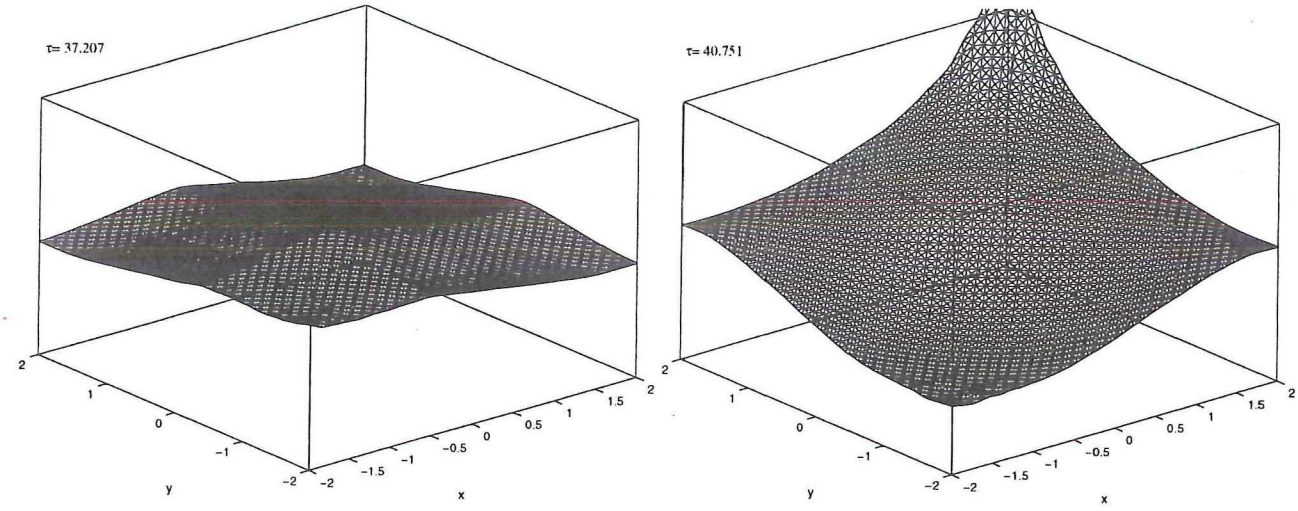

Fig. 13. Snapshots of the free surface for Case B (height of the box = $2d$).

agreement between the analytical and numerical results is found.

The present numerical method is now used to analyse cases with larger amplitude, still with $\omega/\omega_0 \approx 0.999$. We consider the surging motion with $a = 0.0186$, which is ten times larger than that in the previous case. Fig. 6 plots the free surface elevation measured from the bottom of the tank at two time steps, as obtained from the experimental data [5], the linear analytical solution and the non-linear numerical simulation. It can be seen that the numerical simulation gives better agreement with the experimental data, but the linear solution still gives good results in this case.

To further demonstrate the effects of non-linearity, the results for different excitation amplitudes are plotted in Fig. 7, where $\chi = d/L$ and $\omega/\omega_0 \approx 0.999$. It can be observed that with increase of amplitude, the crests become sharper, the troughs become flatter and the period tends to be longer. All these effects have also been noted by Armenio and La Rocca [7] for the two-dimensional roll motion. The gradual increase of the period is also discussed by Greaves [11] and Tsai and Jeng [12] for the case of free oscillation in a tank.

The motion near the first natural frequency ω_0 has some

Table 2
Parameters for convergence study

Case	M_1	M_2	N	$\Delta\tau$
c1	40	40	12	0.0111
c2	80	80	18	0.0111
c3	40	40	12	0.0219

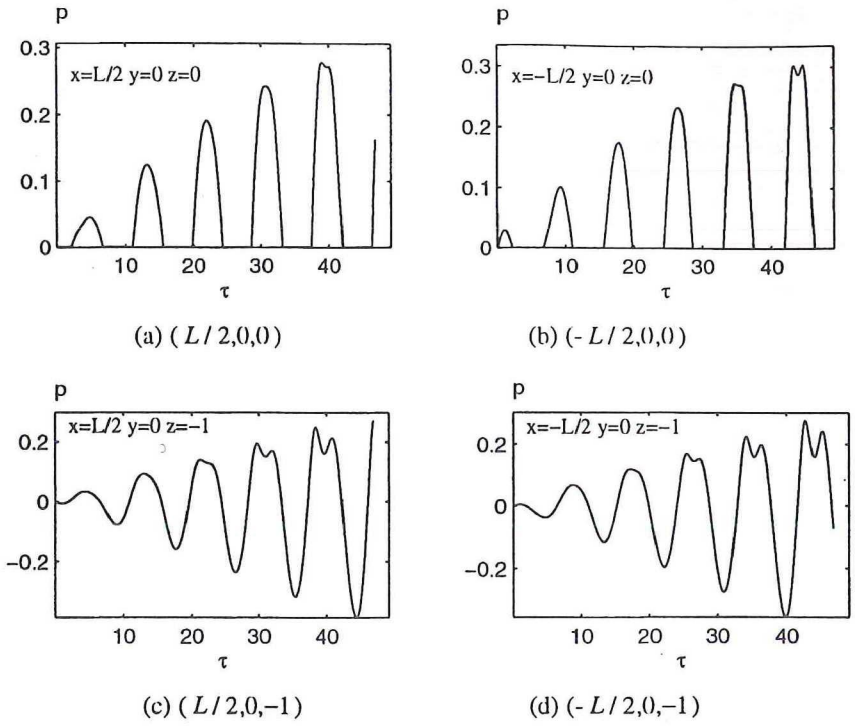

Fig. 14. Pressure history at four points on the tank wall (Case B). (a) (L/2,0,0); (b) ($-L$/2,0,0); (c) (L/2,0, − 1); (d) ($-L$/2,0, − 1).

interesting features. Apart from the normal standing wave, a travelling wave and a bore may exist. Based on their investigation into the two dimensional roll motion, Armenio and La Rocca [7] have mentioned that these three waves may all appear, depending on χ. Huang and Hsiung [8] have also noticed the bore, when using a shallow water formulation.

Our analysis shows the occurrence of a normal standing wave in Fig. 7(b). We now consider two cases, with χ = 0.125, 0.04, to demonstrate a travelling wave and a bore. In the first case, the tank length is taken as $L = 8$. Two different amplitudes of the motion are considered with the same frequency, $\omega = 0.9998\omega_0$. The mesh is generated using $M_1 = 40$, $M_2 = 6$, $N = 16$ and the time step is chosen as $\Delta\tau = 0.0273$. Fig. 8 present the wave profile, wave history and pressure on the side walls for the amplitude $a = 0.0372$. Fig. 8(d) clearly exhibits a wave with one peak travelling in the tank. When the peak reaches the wall, the pressure is apparently larger than the static pressure as shown in Fig.

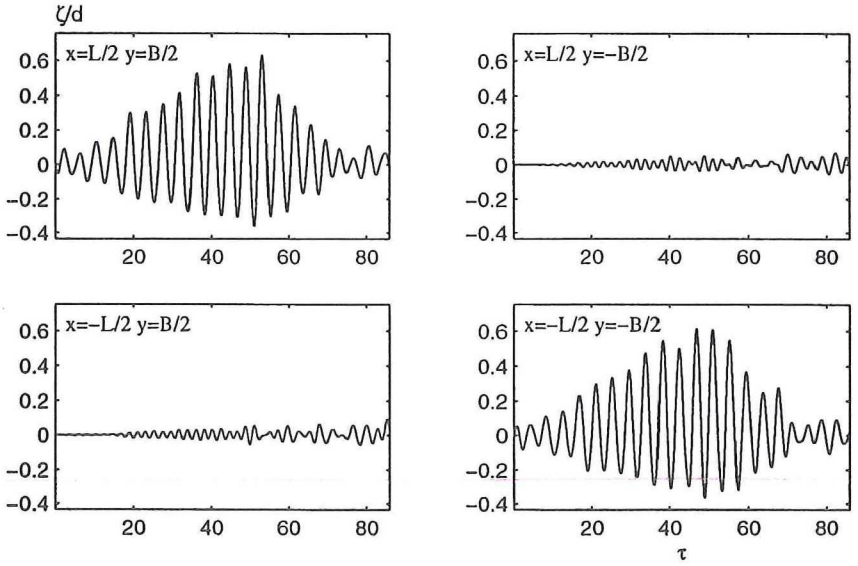

Fig. 15. Wave elevation history at four corners (Case C).

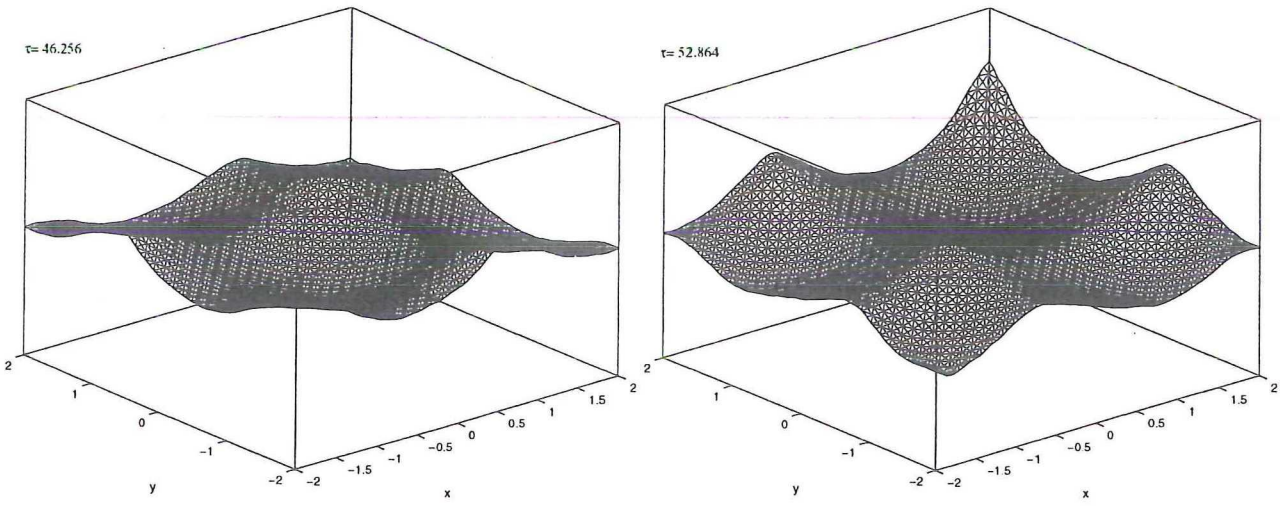

Fig. 16. Snapshots of the free surface for Case C (height of the box = $2d$).

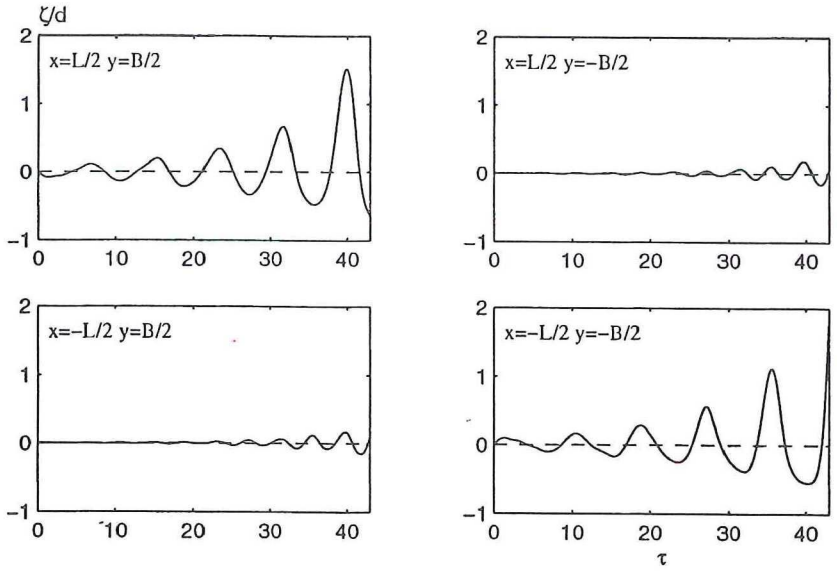

Fig. 17. Wave elevation history at four corners (Case D) (Solid line: u, v given in equation (25); Dashed line: $u = v = 0$).

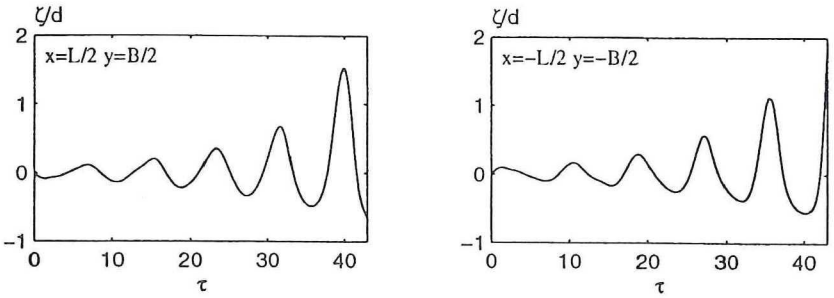

Fig. 18. Wave elevation history at two corners: four lines coincide with each other (Case D, $\omega_z = 0.5\omega_{0x}$, 1.0 ω_{0x}, $1.5\omega_{0x}$ and $2.5\omega_{0x}$, and $a_z\omega_z^2 = 0.428$).

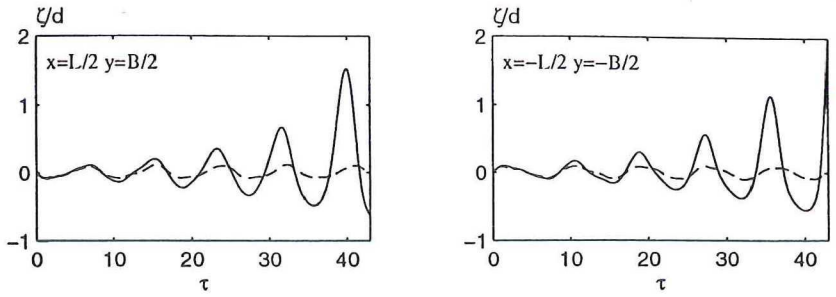

Fig. 19. Wave elevation history at two corners (Case D, $\omega_z = 0.5\omega_{0x}$, Solid line: $a_z\omega_z^2 = 0.428$; Dashed line: $a_z\omega_z^2 = 0.129$).

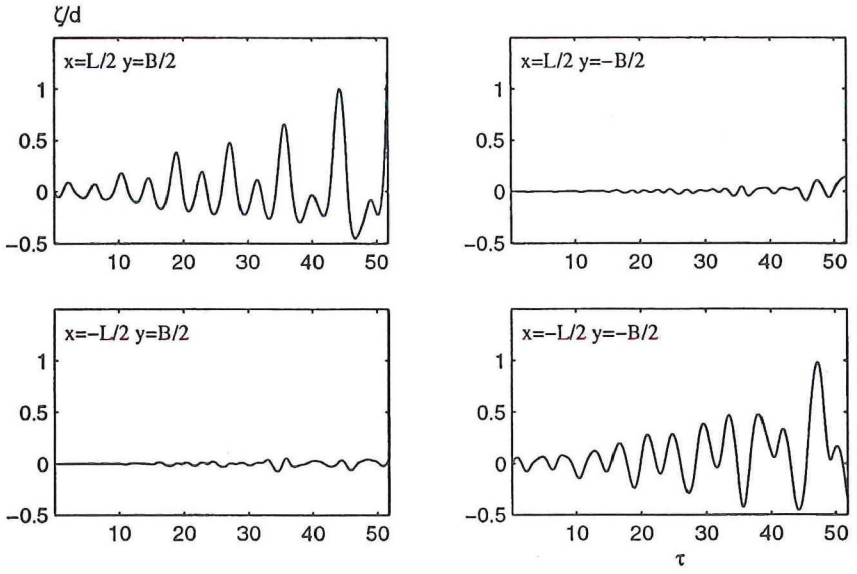

Fig. 20. Wave elevation history at four corners (Case E).

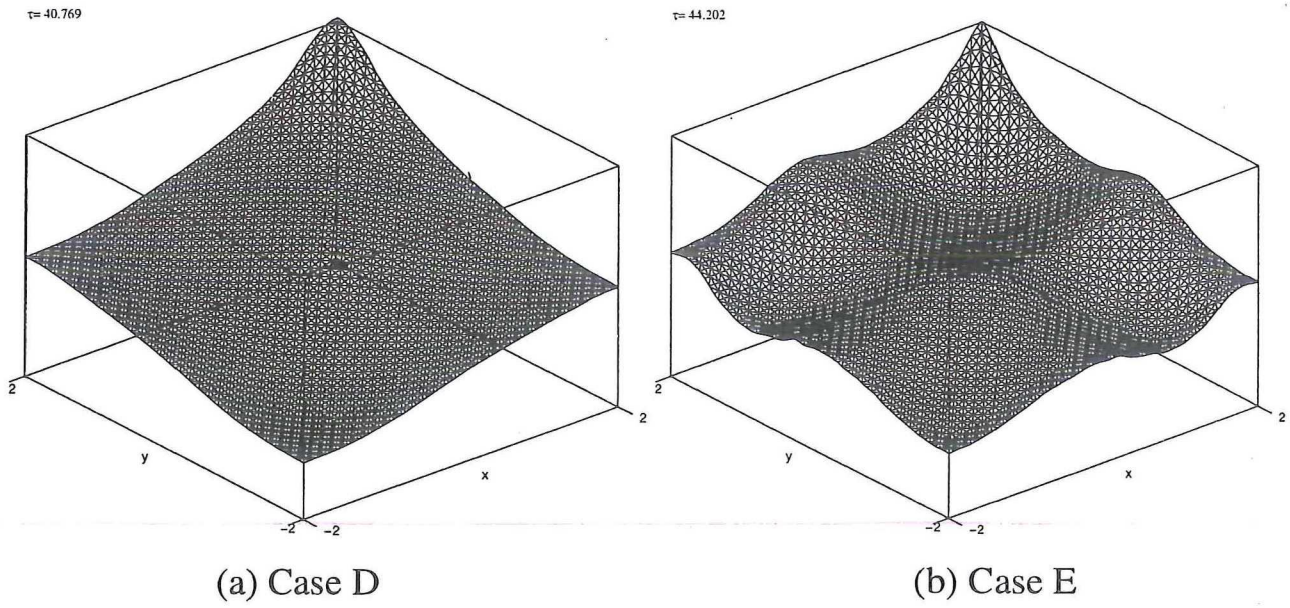

(a) Case D (b) Case E

Fig. 21. Snapshots of wave profile for Case D and Case E (height of the box = $2d$).

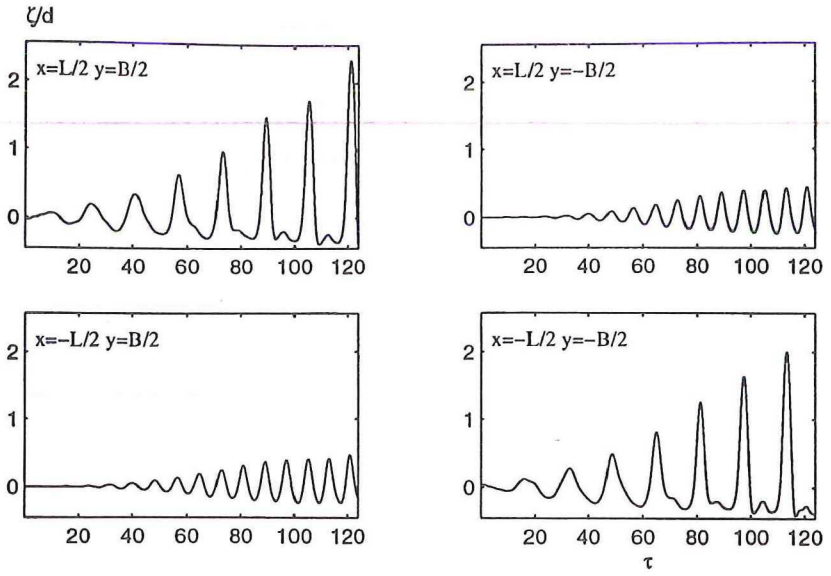

Fig. 22. Wave elevation history at four corners (Case F).

8(b). The travelling wave does not appear immediately after the tank starts to move. Instead, there is a transient period during which the wave changes gradually from standing wave to travelling wave, as illustrated in Fig. 8(c). Fig. 8 also shows that the wave history is very different from that in Fig. 7. The non-linear effects are even more significant and the peaks are even sharper here. The peaks are modulated but the modulation frequency is no longer equal to the difference between the excitation frequency and the first natural frequency ($2\pi/\Delta\omega \approx 8.2 \times 10^5$ from the linear theory).

In the second case, the length is taken as $L = 25$, which corresponds to very shallow water. The excitation frequency is taken as $\omega = 0.9973\omega_0$ and the amplitude $a = 2.5$. The wave profiles are shown in Fig. 9. It can be seen that a bore appears after about $\tau \approx 26$. To the left of the bore, the water surface is almost flat and the free surface elevation is small. To the right of the bore, the wave elevation is much higher. In addition, there is some higher frequency undulation superimposed on the right. This is different from the bore observed by Huang and Hsiung [8] using the shallow water approximation. Their equation is essentially based on the Airy theory, in which there are no dispersive terms to permit modelling of undulations, see Peregrine [13]. In the case here, it is more appropriate to base the shallow water approximation on the Boussinesq equations, which allow waves of relatively short length. Further, in Fig. 9 there is also a period of transition before the bore is formed as in Fig. 8(c). It should be mentioned that the bore has never been observed in our calculation if the motion is very small.

Chester [14] and Chester and Bones [15] have also studied the behaviour of sloshing waves around resonance by an approximate method and by experiments. The results from the two methods were given in separate figures and the comparison seems to be favourable qualitatively. Their data have shown that the history of the wave elevation may have one, two or more peaks within each period, depending on the frequency and amplitude of the excitation, and the depth. In particular, at $\omega = \omega_0$, one peak can be observed when $\chi = 1/12$ and two peaks when $\chi = 1/24$. Fig. 8 and Fig. 9 seem to display some similarity to this kind of behaviour, but our results are not entirely identical to theirs. The difference seems to be mainly due to the fact that the profiles they gave are those in the steady periodic stage, but the modulation still exists in our calculation, even after a long simulation. Further longer simulation is not attempted in this paper, because to reduce the accumulated error, a very fine mesh and small time steps would have to be used, which requires prohibitive computer resources.

4.2. Three dimensional cases

The tank in these cases is subjected to motions defined by $x_b(t) = a_x\sin(\omega_x\tau)$, $y_b(t) = a_y\sin(\omega_y\tau)$ and $z_b(t) = a_z\sin(\omega_z\tau)$ where a_{x_i} and $\omega_{x_i}(x, = x, x_2 = y, x_3 = z)$ are the amplitudes and frequencies in surge, sway and heave modes, respectively. The corresponding velocities are then $u(t) = \omega_x a_x\cos(\omega_x\tau)$, $v(t) = \omega_y a_y\cos(\omega_y\tau)$ and $w(t) = \omega_z a_z\cos(\omega_z\tau)$.

The wave motion in the three dimensional tank is much more complicated than that in the two dimensional case. Several cases with different parameters, as listed in Table 1, are considered below to demonstrate how they influence the waves induced in the tank. ω_{ix} and ω_{iy} $(i = 0,1)$ in the table are the natural frequencies based onthe linear analysis corresponding to the x and y directions. It should be noted that the natural frequencies in the three dimensional cases

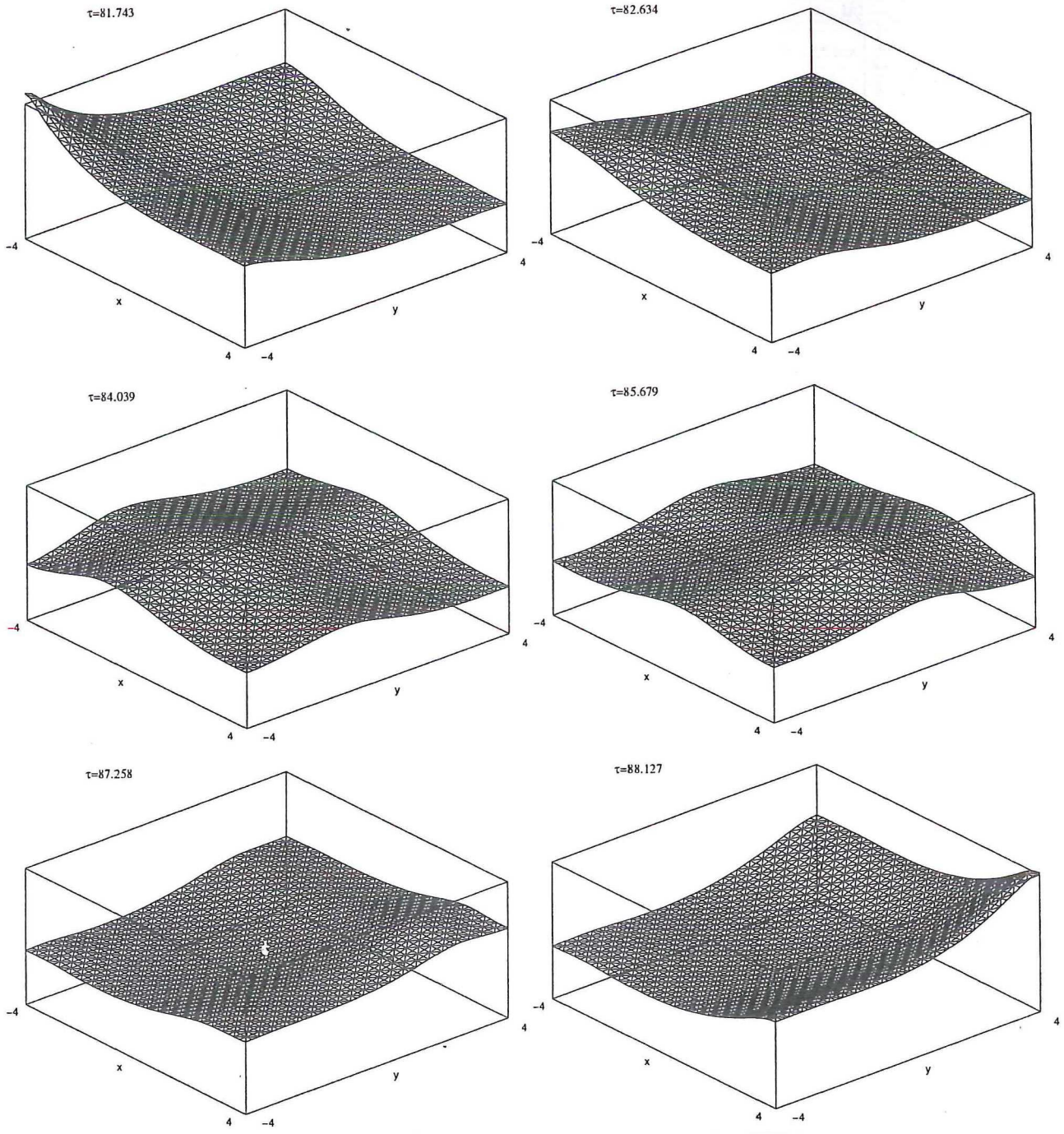

Fig. 23. Snapshots of travelling waves for Case F (height of the box = $2d$).

are

$$\sqrt{\left(\frac{m\pi}{L}\right)^2+\left(\frac{n\pi}{B}\right)^2}\tanh\sqrt{\left(\frac{m\pi}{L}\right)^2+\left(\frac{n\pi}{B}\right)^2}$$

$$(m,n=0,1,2,\ldots)$$

Among them, the terms with $m = 1,3,5\ldots$, $n = 0$ and $n = 1,3,5,\ldots$, $m = 0$ correspond to the symmetric motions in the x and y directions, respectively. Thus the first and second natural frequencies in the x direction, ω_{0x} and ω_{1x} in the table, are obtained by taking $m = 1$, $n = 0$ and $m = 3$, $n = 0$, respectively. Similarly ω_{0y} and ω_{1y} are obtained by taking $m = 0$, $n = 1$ and $m = 0$, $n = 3$, respectively.

Case B is taken as an example for the convergence study. The mesh is generated in a similar way to that shown in Fig. 2. Table 2 lists the parameters used for this examination of convergence, based on the definition of M_1, M_2 and N given in Section 4.1.

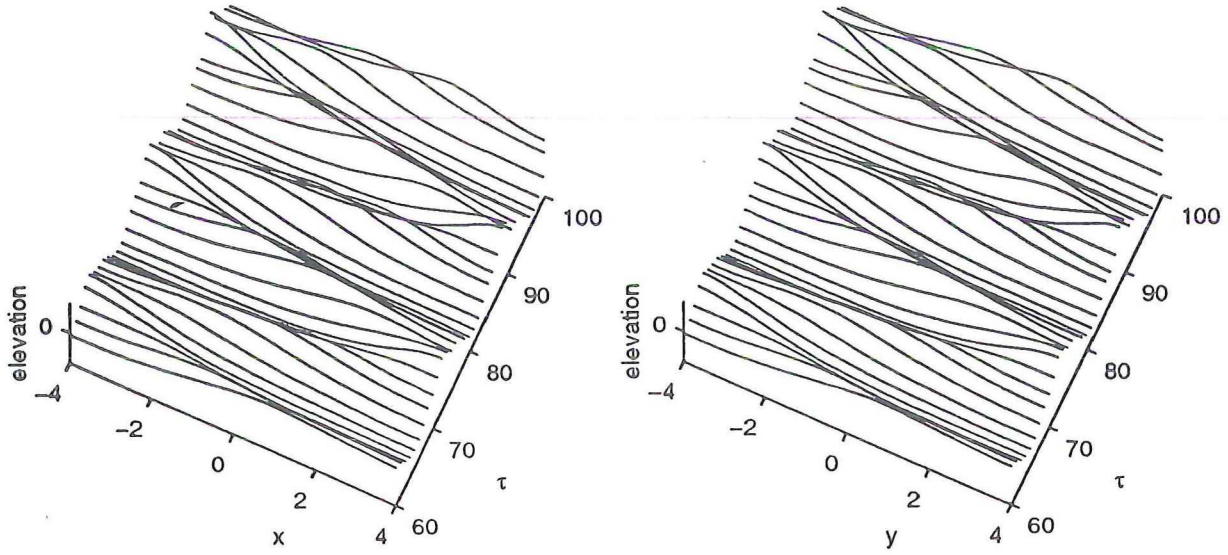

Fig. 24. Wave profiles on two vertical planes (Case F) [(a): on the plane y = 0; (b): on the plane x = 0].

Fig. 10 presents the time history of the free surface elevation for all cases in Table 2, taken at the corner (*L*/2, *B*/2) where the wave is found to be very steep (see Fig. 12). Fig. 10(a) is for cases c1 and c2 where the time steps are the same but the meshes are different; while Fig. 10b is for c2 and c3 where the meshes are the same but the time steps are different. Also plotted in these figures are the differences between c2 and c1, and between c3 and c1. The figures show that the results from these meshes and time steps are in good agreement. This suggests that between 40 to 80 divisions in each wave length and 400 time steps in each wave period are needed to obtain the converged results. But these parameters clearly very much depend on the time period over which the calculation is made and other factors such as the wave amplitude. In the following analysis, these parameters are chosen in such a way that the same degree of accuracy is maintained.

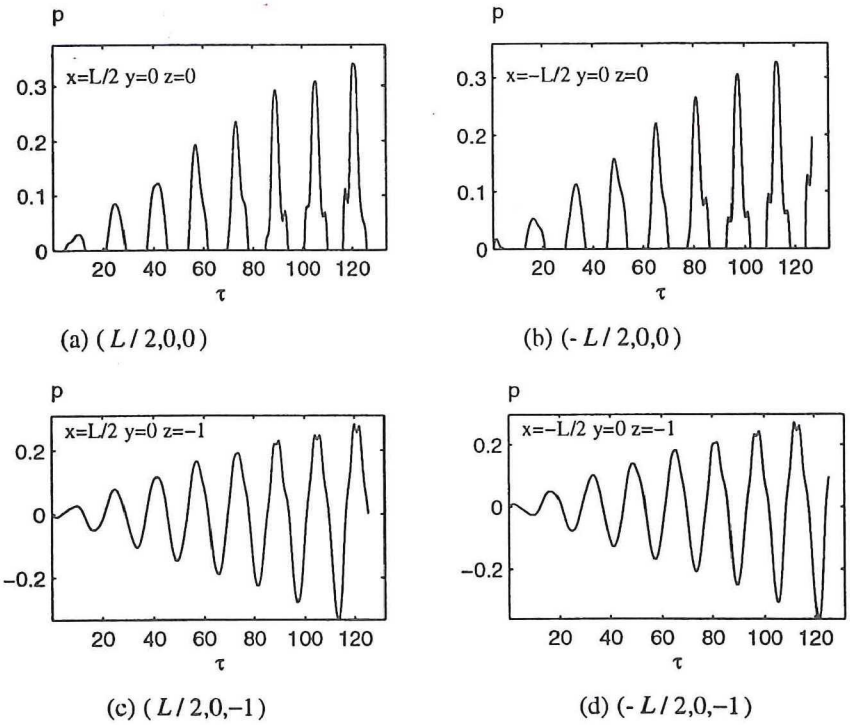

Fig. 25. Pressure history at four points (Case F).

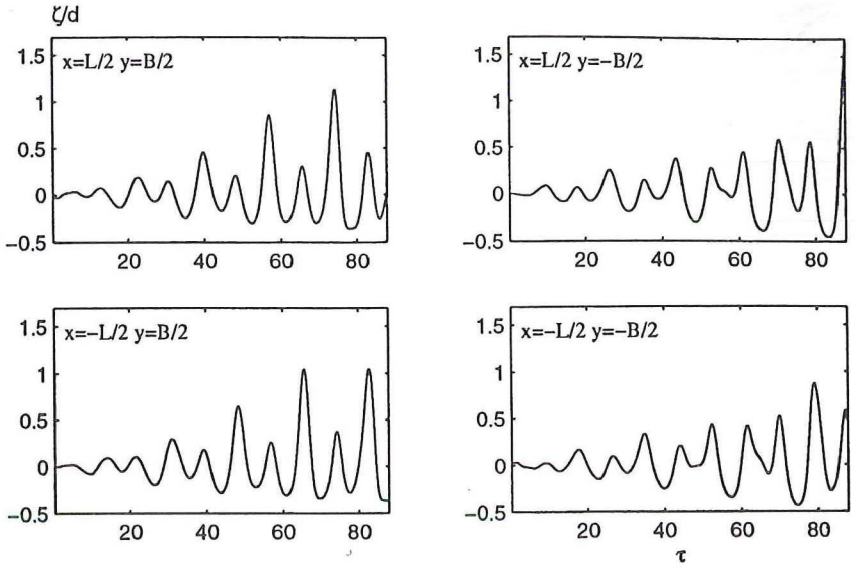

Fig. 26. Elevation history at four corners (Case G).

4.2.1. Sloshing waves in Cases A to E

In all these cases the tank has the same length. The varying parameters are the width, the frequency and the excitation amplitude. In Case A, the motion is very small. The fluid domain is discretised using $M_1 = 40$, $M_2 = 40$ and $N = 12$, and the time step is taken as $\Delta\tau = 0.0146$. The wave elevation histories at the four corners of the tank are given in Fig. 11. It can be seen that the wave amplitude at two corners ($L/2$, $B/2$) and ($-L/2$, $-B/2$) increases with time while the wave elevations at the other two corners are almost zero.

In Case B, the excitation amplitude is one hundred times bigger than that in Case A. Fig. 12 presents the wave elevation history at the four corners. Unlike in Case A, the free surface elevation at corners ($L/2$, $-B/2$) and ($-L/2$, $B/2$) is no longer invisible and, especially after $\tau \approx 20$, the increase of the amplitude with time becomes evident. The peak at the other two corners ($L/2$, $B/2$) and ($-L/2$,$-B/2$) can become quite large, indeed it is about three times bigger than the initial water depth after $\tau \approx 40$.

Two typical snapshots of the free surface are illustrated in Fig. 13, where the height of the plotted box is $2d$. Fig. 14 provides the pressure history (excluding the contribution from the static pressure) recorded at four points: two on the mean free surface and two on the bottom. It shows that as the time progresses, double peaks appear in the time-history of the pressure, which is particularly evident on the bottom. This is very similar to that observed by Nagai [16] in the pressure in steady-state standing waves, and that observed by Cooker et al. [17] in the force on a vertical wall subject to a solitary wave.

In the above two cases the excitation frequency is approximately equal to the first natural frequency of the tank. In Case C, this frequency is increased to near the second natural frequency of the tank. Fig. 15 shows the wave elevations at the four corners. It should be noticed that both the velocity amplitude ($\omega_x a_x$) and the acceleration amplitude ($\omega_x^2 a_x$) of the excitation in this case are larger than those in Case B, but the wave amplitude here is much smaller. The snapshots of the wave elevation are shown in Fig. 16, which shows that the wave is shorter than that in Fig. 13, as expected.

We now consider the cases including the vertical motion. In Case D, the tank oscillates only vertically but with a small initial perturbation of the horizontal velocities. The excitation is defined by:

$$\begin{cases} u(\tau) = v(\tau) = \begin{cases} 0.0283 & \tau = 0 \\ 0 & \tau > 0 \end{cases} \\ w(\tau) = \omega_z a_z \cos(\omega_z \tau) \end{cases}$$

The frequency of the vertical motion is taken to be about twice the first natural frequency in the horizontal direction. The waves generated by the vertical oscillation are called Faraday waves. Benjamin and Ursell [18] explained the mechanism of such waves by analysing Mathieu's equations derived from the linear theory. Since then, a considerable number of papers have been published on this topic, which have been reviewed by Miles and Henderson [19] and Jiang et al. [20]. Here we try to demonstrate the transient behaviour of the Faraday waves.

The mesh for this case is the same as that used in Case B and the time increment is taken as 0.0107. The wave elevations at the four corners are plotted in Fig. 17. The results without a horizontal perturbation (dashed line) are also included in this figure for comparison. It can be seen that the motion of the free surface is not at the excitation frequency but at the first natural frequency of the tank. A similar case was reported by Su and Wang [21], based on their solution of the Navier–Stokes equations. We have investigated

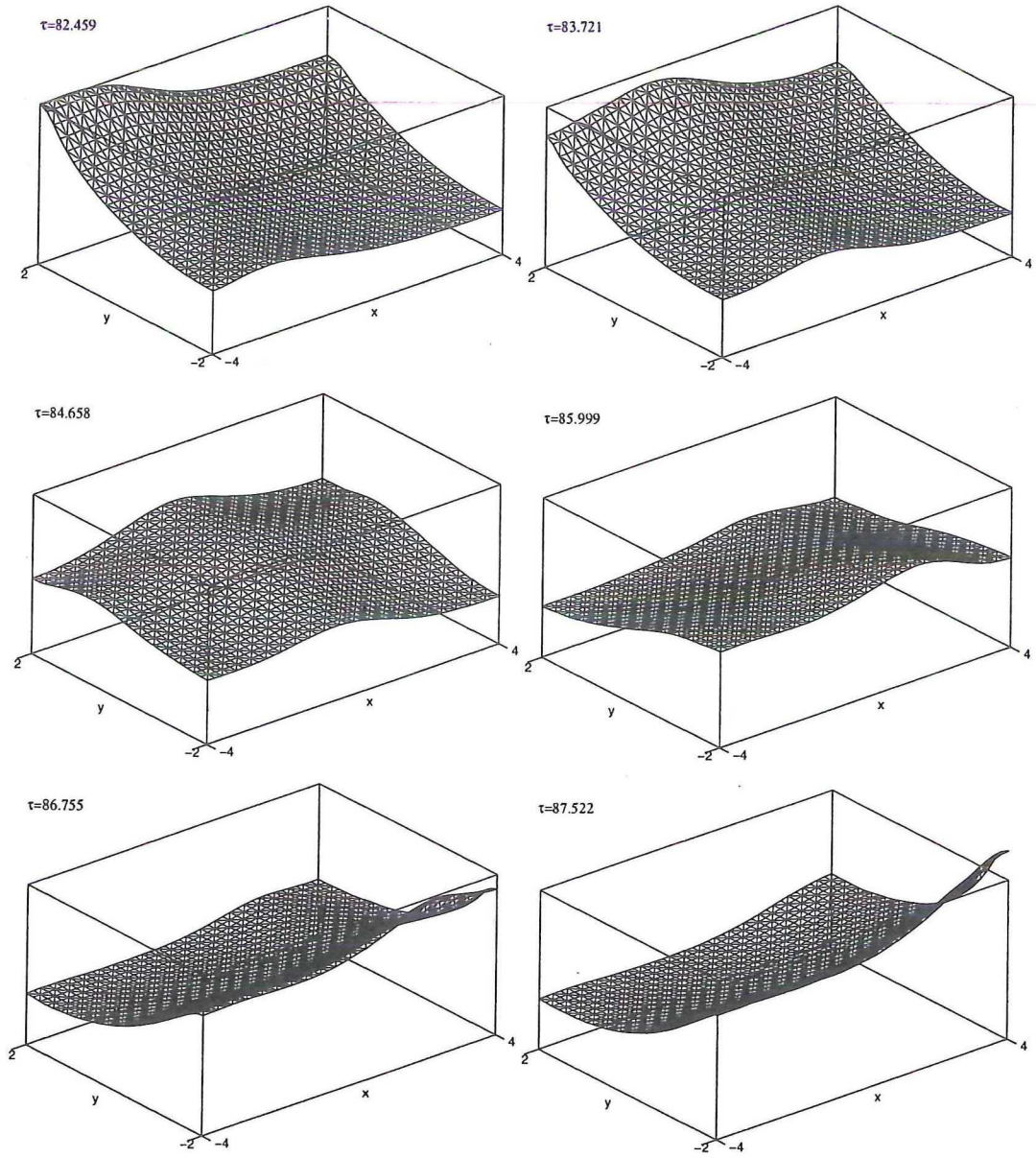

Fig. 27. View of travelling waves for Case G (height of the box = $2d$).

other cases with excitation frequencies $\omega_z = 0.5\omega_{0x}$, $1.0\omega_{0x}$, $1.5\omega_{0x}$ and $2.5\omega_{0x}$ but a fixed acceleration amplitude ($a_z\omega_z^2 = 0.428$ as in Fig. 17) was considered. The results, indicated in Fig. 18, show that the history of the wave elevation in all the cases is almost the same. This suggests that the wave evolution during the transient period generated by the vertical excitation with a given horizontal perturbation may be determined only by the acceleration amplitude of the excitation. To further confirm this, Fig. 19 presents the wave history generated by excitations with the same frequency $\omega_z = 0.5\omega_{0x}$ but different amplitudes, corresponding to $a_z\omega_z^2 = 0.428$ and $a_z\omega_z^2 = 0.129$ respectively. It shows that the results in these cases are very different.

Case E is similar to case D, except that a horizontal excitation is applied throughout the time history. What is interesting here is that despite the horizontal excitation being applied over the entire period of the calculation, the wave amplitudes in this case (as shown in Fig. 20) are no larger than that in Case D (shown in Fig. 17). The comparison of the free surfaces in these two cases is illustrated in Fig. 21. Compared to Case C, where the horizontal motion is the same as that in Case E but with no vertical motion, the amplitude in Case E is much larger.

4.2.2. Sloshing waves in Cases F and G

In these two cases, the water depth is effectively smaller. In Case F, the ratio of depth/length (=depth/width) is set as

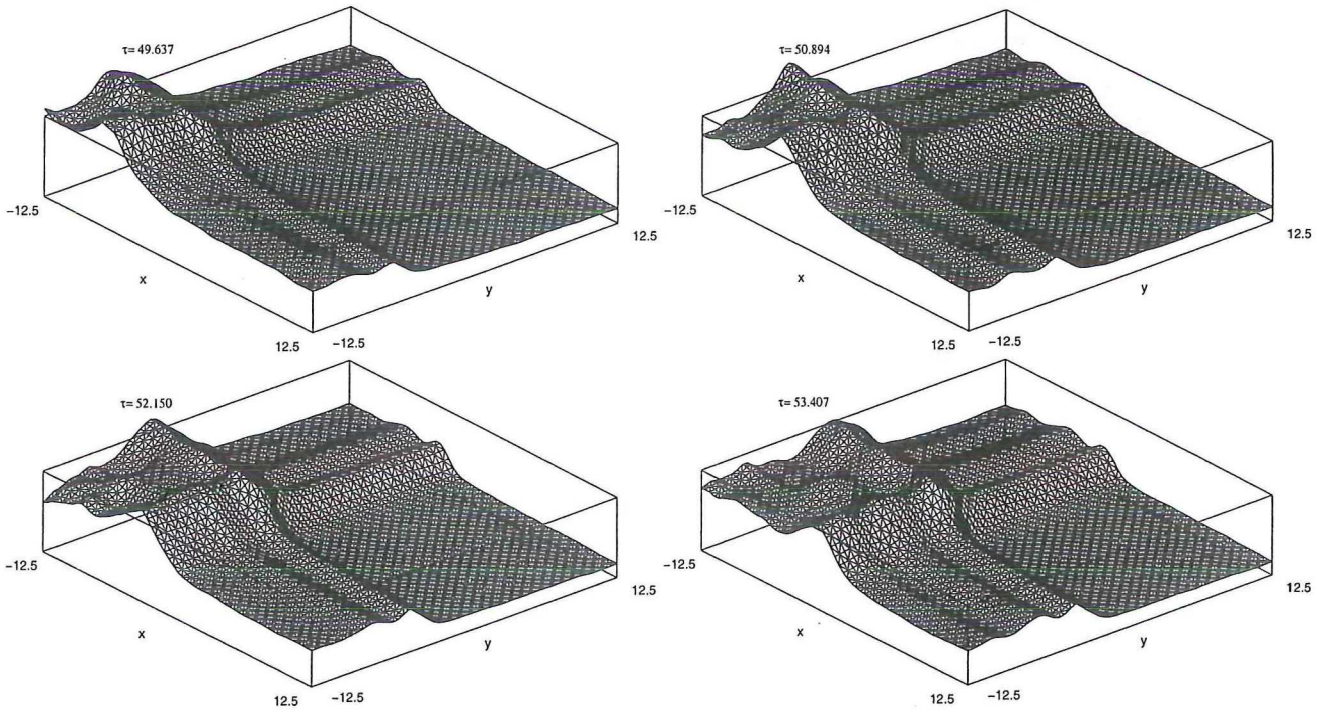

Fig. 28. Surface view of sloshing wave for Case H (height of the box = $2d$)

0.125, which is the same as in the 2D case of Fig. 8 where the travelling wave has been observed. The wave elevation histories at the four corners are shown in Fig. 22. Fig. 23 shows a sequence of a wave crest moving from the corner ($-L/2$, $-$B/2) to the corner ($L/2$, B/2). Fig. 24 gives the profiles on two vertical planes, y=0 and x=0, at different time steps.

These results clearly show that the travelling wave exists in this case. Fig. 25 illustrates the pressure history at four points: two on the mean free surface and two on the bottom. Compared with Fig. 14, the double peaks do not seem to exist in the pressure at the mean free surface, but there are small peaks around the big one. The pressure on the bottom, on the other hand, has similar behaviour to that in Fig. 14.

In the cases considered above, both the tank and the external disturbance are symmetrical about the vertical plane joining the two corners ($L/2$, $B/2$) and ($-L/2$, $-B/2$). The wave motion is therefore also symmetrical. In Case G, the width is reduced by half, and so the property of symmetry no longer exists. The wave elevation history is shown in Fig. 26. The travelling wave is also evident in this case, as shown in Fig. 27. However the water surface can become very high at all corners, instead of just at two corners as in the previous cases.

4.2.3. Sloshing waves for Case H

This is an extremely shallow water case. The tank is undergoing horizontal motion only, at a frequency near to the first natural frequency. As discussed in connection with Fig. 10 for the two dimensional case, a bore may be generated when the water depth is very small. Fig. 28 gives snapshots of the wave profiles for this case. One can see from this figure that the three dimensional bore is travelling from the corner ($-L/2$, $-B/2$) to the corner ($L/2$, $B/2$).

5. Conclusion

This paper has provided extensive results for sloshing waves in a 3D tank undergoing translational motions. The results obtained have confirmed various wave patterns observed in simplified methods. One particular feature noticed in this paper is that the transient waves caused by the vertical oscillation for a given horizontal perturbation depend only on the amplitude of the acceleration of the excitation. Many of results discussed here clearly require further investigation. More work is also needed so that the technique can deal with bottom emergence, impact forces on the top of the tank and wave overturning and breaking. A better understanding of sloshing waves under these conditions will no doubt be invaluable to the many engineering applications discussed in the introduction

Acknowledgements

This work was sponsored by research grant ref. GR/K80372 from the UK Engineering and Physical Sciences Research Council. We also acknowledge the most helpful comments by Professor D.H. Peregrine on an earlier draft of this paper.

References

[1] Abramson HN. The dynamic behaviour of liquid in moving containers. Report SP 106 of NASA, 1996.

[2] Solaas F, Faltinsen OM. Combined numerical solution for sloshing in two-dimensional tanks of general shape. Journal of Ship Research 1997;41:118–129.

[3] Jones AF, Hulme A. The hydrodynamics of water on deck. Journal of Ship Research 1987;31(2):125–135.

[4] Faltinsen OM. A numerical non-linear method of sloshing in tanks with two dimensional flow. Journal of Ship Research 1978;18(4):224–241.

[5] Okamoto T, Kawahara M. Two-dimensional sloshing analysis by Lagragian finite element method. International Journal for Numerical Methods in Fluids 1990;11:453–477.

[6] Chen W, Haroun MA, Liu F. Large amplitude liquid sloshing in seismically excited tanks. Earthquake Engineering and Structural Dynamics 1996;25:653–669.

[7] Armenio V, La Rocca M. On the analysis of sloshing of water in rectangular containers: numerical study and experimental validation. Ocean Engineering 1996;23(8):705–739.

[8] Huang ZJ, Hsiung CC. Nonlinear shallow-water flow on deck. Journal of Ship Research 1996;40(4):303–315.

[9] Wu GX, Ma QW, Eatock Taylor R. Analysis of interactions between non-linear waves and bodies by domain decomposition, ONR 21st Symposium on Naval Hydrodynamics. Trondheim, Norway, 1996.

[10] Ma QW, Wu GX, Eatock Taylor R. Finite element analysis of the non-linear transient waves in three dimensional long tank, in: 12th International Workshop on Water Waves and Floating Bodies. Carry-le-Rouet, France, 1997.

[11] Greaves DM. Numerical modelling of laminar separated flows and inviscid steep waves using adaptive hierarchical meshes, DPhil thesis, Department of Engineering Science, University of Oxford, 1995.

[12] Tsai CP, Jeng DS. Numerical Fourier solution of standing waves in finite water depth. Applied Ocean Research 1994;16:185–193.

[13] Peregrine DH. Calculations of the development of an undular bore. J Fluid Mech 1966;25:321–330.

[14] Chester W. Resonant oscillation of water waves Part I: Theory. Proc Roy Soc Lond 1968;A306:5–22.

[15] Chester W, Bones JA. Resonant oscillation of water waves Part II: Experiment. Proc Roy Soc Lond 1968;A306:23–39.

[16] Nagai S. Pressure of standing waves on vertical walls. J Waterways and Harbour Div ASCE 1969;WW1:53–76.

[17] Cooker MJ, Weidman PD, Bale DS. Reflection of a high-amplitude solitary wave at a vertical wall. J Fluid Mechanics 1997;342:141–158.

[18] Benjamin TB, Ursell F. The stability of the plane free surface of a liquid in vertical periodic motion. Proc Roy Soc Lond 1954;A225:505–515.

[19] Miles JW, Henderson DM. Parametrically forced surface waves. Ann Rev Fluid Mech 1990;22:143–165.

[20] Jiang L, Ting CL, Perlin M, Schultz W. Moderate and steep Faraday waves: instabilities, modulation and temporal asymmetries. J Fluid Mech 1996;329:275–307.

[21] Su TC, Wang Y. Numerical simulation of three-dimensional large amplitude liquid sloshing in rectangular containers subjected to vertical excitation. In: Seismic Engineering for Piping Systems, Tanks and Power Plant Equipment, vol. 108. ASME, 1986:149–154.